



The Ekman spiral for piecewise-uniform diffusivity

David G. Dritschel¹, Nathan Paldor², Adrian Constantin³

¹School of Mathematics and Statistics, University of St Andrews,
St Andrews KY16 9SS, UK

²The Fredy & Nadin Herrman Institute of Earth Sciences, The Hebrew University,
Jerusalem 9190401, Israel

³Department of Mathematics, University of Vienna,
Vienna 1090, Austria

May 13, 2020

Abstract

We re-visit Ekman's (1905) classic problem of wind-stress induced ocean currents to help interpret observed deviations from Ekman's theory, in particular from the predicted surface current deflection of 45° . While previous studies have shown that such deviations can be explained by a vertical eddy viscosity varying with depth, as opposed to the constant profile taken by Ekman, analytical progress has been impeded by the difficulty in solving Ekman's equation. Herein, we present a solution for piecewise-constant eddy viscosity which enables a comprehensive understanding of how the surface deflection angle depends on the vertical profile of eddy viscosity. For two layers, the dimensionless problem depends only on the depth of the upper layer and the ratio of layer viscosities. A single diagram then allows one to understand the dependence of the deflection angle on these two parameters.

1 Introduction

The motion of the near-surface ocean layer is a superposition of waves, wind-driven currents and geostrophic flows. The basic theory of wind-driven surface currents in the ocean, away from the Equator, is due to Ekman (1905) and constitutes a cornerstone of oceanography (see Vallis, 2017). Ekman dynamics is due to the balance between Coriolis and the frictional forces generated by the wind stress. Its main features, consistent with observations of steady wind-driven ocean currents, are:

- (i) the surface current is deflected to the right/left of the prevailing wind direction (in the Northern/Southern Hemisphere);
- (ii) with increasing depth in the boundary layer, the current speed is reduced, and the direction rotates farther away from the wind direction following a spiral;
- (iii) the net transport is at right angles to the wind direction, to the right/left of the wind direction in the Northern/Southern Hemisphere.

While near the Equator wind-drift currents move in the same direction as the wind (see the discussion in Boyd, 2018), away from the Equator a deflection of steady wind-driven currents



with respect to the prevailing wind direction occurs in a surface boundary layer, whose typical depth is tens of metres. Ekman's pioneering solution (see Ekman, 1905), derived for a constant vertical eddy viscosity, captures the general qualitative behaviour, but differences of detail between observations and Ekman theory were recorded in the last decades. While the characteristics (ii)-(iii) hold for any depth-dependent vertical eddy viscosity (see Constantin, 2020), there is a need to explain the occurrence of surface currents at an angle in the range 10-75° to the wind (rather than the 45° predicted by Ekman), with large variations depending on the regional and seasonal climate (see the data in Röhrs and Christensen, 2015; Yoshikawa and Masuda, 2009).

This discrepancy is typically ascribed to the effect of a vertical eddy viscosity that varies with depth. The explicit solution found by Madsen (1977), for a vertical eddy viscosity that varies linearly with depth, leads to a plausible, although somewhat low, surface current deflection angle of about 10°. The avenue of seeking explicit solutions is not very promising, since only a few are available and the intricacy of the details makes it difficult to extract broad conclusions (we refer to Constantin and Johnson, 2019; Grisogno, 1995, for a survey of known Ekman-type solutions). The challenging nature of the task is highlighted by the recent analysis pursued in Bressan and Constantin (2019); Constantin (2020) where asymptotic approaches, applicable for eddy viscosities that are small perturbations of a constant, revealed the convoluted way in which the eddy viscosity influences the deflection angle: while a slow and gradual variation of the eddy viscosity with depth results in a deflection angle larger than 45°, the typical outcome of an eddy viscosity concentrated in the middle of the boundary layer is a deflection angle below 45°. A better understanding of the deflection angle is important theoretically but also for operational oceanography, e.g. in the context of search-and-rescue operations or in remedial action for oil spills.

The important issue of a quantitative relation between the vertical eddy viscosity and the magnitude of the deflection angle remains open. The aim of this paper is to discuss this issue in cases when the eddy viscosity is piecewise uniform. The in-depth analysis that can be pursued in this relatively simple setting permits us to gain insight into the way the turbulent parametrization (e.g. of general circulation models) controls the deflection angle. This paper is organised as follows: in Section 2 we present the Ekman equations for wind-driven ocean for depth-dependent eddy viscosities and we perform a suitable scaling that reduces the number of parameters. In Section 3, an explicit solution is constructed and illustrated for an infinitely-deep ocean with two constant values of eddy viscosity. This solution covers the full range of possibilities, and exhibits deflection angles covering the full range between 0 and 90°. Various special or limiting cases are highlighted. Finally, Section 4 offers our conclusions.

2 Equations of motion and scaling

For a deep, vertically homogeneous ocean, of infinite lateral extent, the horizontal momentum equation for steady flow takes the following (complex) form under the f -plane approximation:

$$if\mathbf{U} = \frac{1}{\rho} \frac{\partial \boldsymbol{\tau}}{\partial Z} - \frac{1}{\rho} \nabla P + \text{higher-order terms}, \quad (1)$$

where $\mathbf{U}(Z) = U + iV$ is the complex horizontal velocity in the (X, Y) -plane, Z is the depth below the mean surface $Z = 0$, f is the Coriolis parameter, ρ is the (constant) density, $\nabla P = \partial P / \partial X + i \partial P / \partial Y$ is the horizontal pressure gradient, $\boldsymbol{\tau}(Z) = \tau_x + i\tau_y$ is the shear stress due to molecular and turbulent processes, and the higher-order terms, representing interactions between the variables, are presumed to be small. Decomposing the horizontal velocity into pressure-driven (geostrophic) and wind-driven (Ekman) components $\mathbf{U} = \mathbf{U}_g + \mathbf{U}_e$, we see from



81 (1) that the leading-order geostrophic and wind-driven flows separate, with the linear equation

$$\text{if } \mathbf{U}_e = \frac{1}{\rho} \frac{\partial \boldsymbol{\tau}}{\partial Z} \quad (2)$$

82 governing the dynamics of the wind-driven flow. By relating the stress vector within the fluid,
 83 $\boldsymbol{\tau}$, to the shear profile through a turbulent eddy viscosity coefficient $\nu(Z)$,

$$\boldsymbol{\tau} = \rho \nu \frac{\partial \mathbf{U}_e}{\partial Z}, \quad (3)$$

84 from (2) we obtain Ekman's equations for wind-driven ocean currents

$$\text{if } \mathbf{U}_e = \frac{\partial}{\partial Z} \left(\nu \frac{\partial \mathbf{U}_e}{\partial Z} \right). \quad (4)$$

85 Let us now discuss the appropriate boundary conditions. At the surface, the shear stress
 86 balances the wind stress, $\boldsymbol{\tau}_0$:

$$\boldsymbol{\tau}_0 = \rho \nu \frac{\partial \mathbf{U}_e}{\partial Z} \quad \text{on } Z = 0. \quad (5)$$

87 The “bottom” boundary condition expresses the vanishing of the wind-driven current with
 88 depth (necessary to keep the total kinetic energy finite), where the flow is essentially geostrophic:

$$\mathbf{U}_e \rightarrow 0 \quad \text{as } Z \rightarrow -\infty. \quad (6)$$

89 Letting τ_0 denote the magnitude of the surface wind stress, we non-dimensionalise the
 90 problem by scaling \mathbf{U}_e on $\sqrt{2\tau_0/\rho}$ and Z on $\sqrt{2\tau_0/\rho}/f$, since τ_0/ρ has units of L^2/T^2 . The
 91 factor of 2 is introduced for convenience below. Upon defining a dimensionless eddy viscosity
 92 $K = f\rho\nu/\tau_0$, velocity $\mathbf{u} = \mathbf{U}_e/\sqrt{2\tau_0/\rho}$ and depth $z = Zf/\sqrt{2\tau_0/\rho}$, the equations transform to

$$(K\psi)' - 2i\psi = 0 \quad \text{for } z < 0, \quad (7)$$

$$\psi'(0) = 1 \quad \text{on } z = 0, \quad (8)$$

$$\psi \rightarrow 0 \quad \text{as } z \rightarrow -\infty, \quad (9)$$

93 where $\psi = \mathbf{u}K(0)$ (cf. equations (14)–(16) in Gill, 1982). The scaling performed does not
 94 change the surface deflection angle θ_0 , equal to the argument of the complex vector $\psi(0)$, even
 95 if the scaling results in an orientation of the horizontal axes such that the surface wind stress
 96 points in the positive x -direction. Finally, we note that this formulation is appropriate for the
 97 Northern Hemisphere where $f > 0$. The formulation for the Southern Hemisphere is obtained
 98 by taking the complex conjugate in (7), noticing that K is real-valued.

99 3 Exact solution for piecewise-constant eddy viscosity

100 For piecewise-constant K , without loss of generality we can further scale z so that $K = 1$ in
 101 $z \in [-h, 0]$ while $K = \ell^2$ in $z \in (-\infty, -h)$, where h is the dimensionless depth of the upper
 102 layer. Note, ℓ is the ratio of the lower-layer to upper-layer viscous lengths. The analysis below
 103 can be readily extended to any number of regions of constant K , but the simplest to understand
 104 is two regions, since then the solution depends on only two dimensionless parameters, ℓ and h .



105 3.1 Constructing the solution

106 In each region, the complex velocity ψ satisfies a simple constant-coefficient equation

$$\psi'' - 2i\psi = 0 \quad \text{for} \quad -h < z < 0, \quad (10)$$

$$\ell^2 \psi'' - 2i\psi = 0 \quad \text{for} \quad -\infty < z < -h, \quad (11)$$

107 having exponential solutions

$$\psi(z) = A e^{(1+i)z} + B e^{-(1+i)z} \quad \text{for} \quad -h < z < 0, \quad (12)$$

$$\psi(z) = C e^{(1+i)z/\ell} \quad \text{for} \quad -\infty < z < -h, \quad (13)$$

108 where A , B and C are (generally complex) constants. The boundary condition $\psi \rightarrow 0$ as
 109 $z \rightarrow -\infty$ has been used to eliminate the growing solution in (13).

110 At the discontinuity in K , at $z = -h$, we require continuity of ψ , i.e. $\psi(-h^+) = \psi(-h^-)$.
 111 Moreover, by integrating the equation above across an infinitesimal region centred on $z = -h$,
 112 we obtain

$$\psi'(-h^+) = \ell^2 \psi'(-h^-). \quad (14)$$

113 The upper surface boundary condition $\psi'(0) = 1$ implies

$$(1+i)(A-B) = 1 \quad (15)$$

114 while continuity of ψ at $z = -h$ implies

$$A e^{-(1+i)h} + B e^{(1+i)h} = C e^{-(1+i)h/\ell} \quad (16)$$

115 and finally the jump condition (14) on ψ' at $z = -h$ implies

$$A e^{-(1+i)h} - B e^{(1+i)h} = C \ell e^{-(1+i)h/\ell}. \quad (17)$$

116 It follows that

$$A = \frac{1}{2} C e^{-(1+i)h/\ell} (1+\ell) e^{(1+i)h} \quad \text{and} \quad B = \frac{1}{2} C e^{-(1+i)h/\ell} (1-\ell) e^{-(1+i)h}. \quad (18)$$

117 Applying the surface boundary condition (15) determines C as

$$C = \frac{(1-i) e^{(1+i)h/\ell}}{(1+\ell) e^{(1+i)h} - (1-\ell) e^{-(1+i)h}}. \quad (19)$$

118 The surface current deflection angle, θ_0 , measured clockwise, is determined from

$$\tan \theta_0 = -\frac{\Im(\psi(0))}{\Re(\psi(0))} = -\frac{\Im(A+B)}{\Re(A+B)}. \quad (20)$$

119 But given C above in (19), we have

$$A+B = \frac{1}{2}(1-i) \frac{(1+\ell) e^{(1+i)h} + (1-\ell) e^{-(1+i)h}}{(1+\ell) e^{(1+i)h} - (1-\ell) e^{-(1+i)h}}.$$

120 Introducing the real values $\alpha = (1+\ell) e^h$ and $\beta = (1-\ell) e^{-h}$ enables us to write

$$A+B = \frac{1}{2}(1-i) \frac{\alpha e^{ih} + \beta e^{-ih}}{\alpha e^{ih} - \beta e^{-ih}}$$

121 which, after multiplying top and bottom by the complex conjugate of the denominator, simpli-
 122 fies to

$$A+B = \frac{1}{2}(1-i) \frac{\alpha^2 - \beta^2 - 2i\alpha\beta \sin(2h)}{\alpha^2 + \beta^2 - 2\alpha\beta \cos(2h)}.$$

123 Hence, taking the (negative of the) ratio of the imaginary to real parts of this, we obtain

$$\tan \theta_0 = \frac{\alpha^2 - \beta^2 + 2\alpha\beta \sin(2h)}{\alpha^2 - \beta^2 - 2\alpha\beta \sin(2h)}. \quad (21)$$



124 3.2 Results

125 First, we examine certain special cases.

126 When $\ell = 1$, there is no discontinuity in eddy viscosity. Since in this case $\beta = 0$, we have
127 $\tan \theta_0 = 1$, i.e. $\theta_0 = 45^\circ$ in agreement with the classical Ekman spiral solution.

128 As $\ell \rightarrow 0$, the eddy viscosity vanishes in the lower layer, and the flow field ψ must also
129 vanish. In this case, $\tan \theta_0$ reduces to

$$\tan \theta_0 = \frac{\sinh(2h) + \sin(2h)}{\sinh(2h) - \sin(2h)}, \quad (22)$$

130 which has a non-trivial dependence on h . The maximum value is attained as $h \rightarrow 0$; then
131 $\tan \theta_0 \rightarrow \infty$ or $\theta_0 \rightarrow 90^\circ$.

132 As $\ell \rightarrow \infty$, corresponding to an extremely viscous lower layer, $\tan \theta_0$ reduces to the inverse
133 of the previous expression, i.e.

$$\tan \theta_0 = \frac{\sinh(2h) - \sin(2h)}{\sinh(2h) + \sin(2h)}. \quad (23)$$

134 The minimum occurs for $h \rightarrow 0$ and there $\tan \theta_0 \rightarrow 0$ or $\theta_0 \rightarrow 0$.

135 For general ℓ , there are also values of h for which $\tan \theta_0 = 1$. These occur when the
136 numerator and the denominator of the general expression above for $\tan \theta_0$ are equal. But this
137 means $\alpha\beta \sin(2h) = 0$ or $(1 - \ell^2) \sin(2h) = 0$. One solution is the classical Ekman spiral with
138 $\ell = 1$ noted above. But we also have $h = n\pi/2$ for non-negative integers n . When $n = 0$,
139 the upper layer vanishes and the eddy viscosity is uniform throughout the entire depth. The
140 classical Ekman spiral is expected in this case. The other special depths imply θ_0 exhibits a
141 non-monotonic dependence on h for fixed ℓ . In fact, θ_0 exhibits a decaying oscillation about a
142 value of unity.

143 A summary of the results in the ℓ - h plane is provided in figure 1. Along any line $\ell = \text{constant}$
144 (excluding $\ell = 1$), θ_0 reaches a minimum or maximum in h when the following relation holds:

$$\frac{1 - \ell}{1 + \ell} = \pm e^{2h} \sqrt{\frac{\cos(2h) - \sin(2h)}{\cos(2h) + \sin(2h)}} \quad (24)$$

145 obtained by setting the partial derivative of $\tan \theta_0$ w.r.t. h equal to zero. The first extremum
146 with increasing h occurs for $h < \pi/8$ (when $h = \pi/8$ the above equation yields $\ell = 1$). Note
147 that as $h \rightarrow 0$, $(1 - \ell)/(1 + \ell) \rightarrow \pm 1$, implying either $\ell \rightarrow 0$ or $\ell \rightarrow \infty$ as noted previously.
148 Extrema also occur for larger h since the function in the square root above is periodic, but
149 these involve much weaker variations in θ_0 about 45° , diminishing like $e^{-n\pi}$ for positive integers
150 n . When $n = 1$, the maximum excursion in $\tan \theta_0$ is approximately 0.05735.

151 4 Conclusions

152 We have re-visited the famous problem originally posed by Nansen (see the discussion in Hunt-
153 ford (2002)) and solved by Ekman (1905) to understand wind-driven currents in the ocean. By
154 balancing viscous and Coriolis forces, and assuming a constant vertical eddy viscosity, Ekman
155 (1905) predicted that the surface current is deflected by 45° to the right/left of the prevailing
156 wind direction (in the Northern/Southern Hemisphere). Moreover, Ekman (1905) found that
157 the net fluid transport is 90° to the right/left of the wind direction.

158 Since then, a number of studies have sought to explain observed discrepancies with Ekman's
159 theory (Röhrs and Christensen, 2015; Yoshikawa and Masuda, 2009), in particular deflection
160 angles significantly different from the 45° prediction (Madsen, 1977; Grisogno, 1995; Bressan
161 and Constantin, 2019; Constantin and Johnson, 2019; Constantin, 2020). The main conclusion

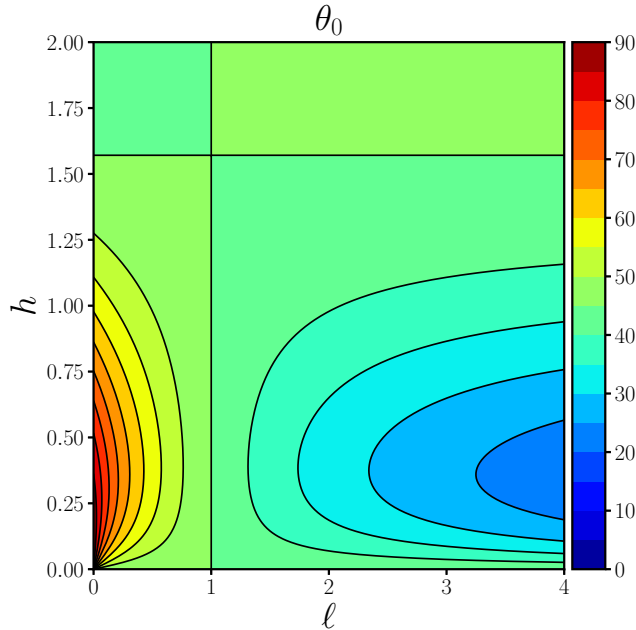


Figure 1: Surface deflection angle θ_0 (in degrees) as a function of the lower-layer non-dimensional viscous length ℓ and the non-dimensional depth of the upper layer h .

162 is that these discrepancies can be explained by vertically-varying eddy viscosities. However,
 163 due to the mathematical difficulty in constructing exact or asymptotic solutions, no general
 164 picture has yet emerged relating the deflection angle to the profile of eddy viscosity.

165 This study makes a first step in this direction by considering the case of piecewise-constant
 166 eddy viscosities for which analytical solutions may be readily constructed and analysed. We
 167 have presented results for the simplest situation of two regions having different uniform viscosi-
 168 ties in an infinitely deep ocean (in fact the results also apply when the two regions have different
 169 densities, such as a mixed layer overlying a denser deep layer). By an appropriate scaling of
 170 the governing equations, the solutions can be shown to depend on only two parameters: the
 171 ratio of the lower-to-upper viscous lengths ℓ and the dimensionless depth of the upper layer h .
 172 This permits one to see at a glance how both ℓ and h determine the surface deflection angle θ_0 .

173 In appropriate limits, we recover Ekman’s classical solution, but additionally the 45° de-
 174 flection angle may *also* occur for arbitrary ℓ , when h assumes special values. In general, for h
 175 sufficiently small and $\ell < 1$ (a less viscous lower layer), the deflection angle exceeds 45° (and
 176 can reach nearly 90° for $\ell \ll 1$). When $\ell > 1$ (a more viscous lower layer), the deflection
 177 angle is less than 45° , and tends to zero as $\ell \rightarrow \infty$ for $h \ll 1$. For $\ell \sim 1$ our conclusions are
 178 in agreement with the results obtained recently in Bressan and Constantin (2019); Constantin
 179 (2020). Indeed, writing $K(z) = \ell^2 + \varepsilon K_1(z)$ for $z \leq 0$, with $\varepsilon = |1 - \ell^2|$ and

$$K_1(z) = \begin{cases} (1 - \ell^2)/\varepsilon, & z \in [-h, 0], \\ 0, & z < -h, \end{cases}$$

180 the perturbative approach developed in Bressan and Constantin (2019); Constantin (2020)
 181 shows that a positive/negative value of the integral

$$\frac{1 - \ell^2}{\varepsilon} \int_{-h}^0 e^{2s} \sin\left(2s + \frac{\pi}{4}\right) ds,$$



182 corresponds to a deflection angle larger/smaller than 45° . The relation

$$\int_{-h}^0 e^{2s} \sin\left(2s + \frac{\pi}{4}\right) ds = \frac{1}{2\sqrt{2}} e^{-2h} \sin(2h)$$

183 shows that this is consistent with our conclusions.

184 The results obtained may help better formulate appropriate parametrisations of eddy vis-
185 cosities in global circulation models of the ocean. For example, it is typical for the upper
186 100 m of the ocean that solar heating quenches turbulence during the day (see the discussion
187 in Woods, 2002). Our model captures these changes: during the day we set $\ell > 1$, with $\ell < 1$
188 during the night, thus explaining the observation that often the deflection angle exceeds 45°
189 during the day, and is below 45° during the night (see Krauss, 1993). The same reasoning
190 applies to the large seasonal variations of the deflection angle observed at some locations (see
191 the data in Yoshikawa and Masuda, 2009) and explains why one observes angles below 45° in
192 arctic regions, where the ice cover quells the turbulence near the ocean surface. On the other
193 hand, the regularity of strong winds in the Drake Passage makes the assumption of a uniform
194 eddy viscosity reasonable (that is, $\ell = 1$), so that in this region the deflection angle is typically
195 close to 45° (see the data in Polton *et al.*, 2013; Roach *et al.*, 2015).

196 References

- 197 Boyd, J. P., *Dynamics of the equatorial ocean*, 2018 (Springer: Berlin).
- 198 Bressan, A. and Constantin, A., The deflection angle of surface ocean currents from the wind
199 direction. *J. Geophys. Res.: Oceans* 2019, **124**, 7412–7420.
- 200 Constantin, A., Frictional effects in wind-driven ocean currents. *Geophys. Astrophys. Fluid*
201 *Dyn.* (in print), doi.org/10.1080/03091929.2020.1748614.
- 202 Constantin, A. and Johnson, R. S., Atmospheric Ekman flows with variable eddy viscosity.
203 *Boundary-Layer Meteorology* 2019, **170**, 395–414.
- 204 Ekman, V. W., On the influence of the Earth’s rotation on ocean-currents. *Ark. Mat. Astron.*
205 *Fys.* 1905, **2**, 1–52.
- 206 Gill, A. E., *Atmosphere-Ocean Dynamics*, 1982 (Academic Press), 662pp.
- 207 Grisogno, B., A generalized Ekman layer profile with gradually varying eddy diffusivities. *Quart.*
208 *J. Roy. Meteorol. Soc.* 1995, **121**, 445–453.
- 209 Huntford, R., *Nansen: The explorer as hero*, 2002 (Abacus).
- 210 Krauss, W., Ekman drift in homogeneous water. *J. Geophys. Res.* 1993, **98**, 187–209.
- 211 Madsen, O. S., A realistic model of the wind-induced Ekman boundary layer. *J. Phys.*
212 *Oceanogr.* 1977, **7**, 248–255.
- 213 Polton, J. A., Lenn, Y.-D., Elipot, S., Chereskin, T. K., and Sprintall, J., Can Drake Passage
214 observations match Ekman’s classic theory? *J. Phys. Oceanogr.* 2013, **43**, 1733–1740.
- 215 Roach, C. J., Phillips, H. E., Bindoff, N. L., and Rintoul, S. R., Detecting and characterizing
216 Ekman currents in the Southern Ocean. *J. Phys. Oceanogr.* 2015, **45**, 1205–1223.
- 217 Röhrs, J., and Christensen, K. H., Drift in the uppermost part of the ocean. *Geophys. Res.*
218 *Lett.* 2015, **42**, 10349–10356.
- 219 Vallis, G. K., *Atmospheric and oceanic fluid dynamics*, 2017 (Cambridge University Press).
- 220 Woods, J., Laminar flow in the ocean Ekman layer. In *Meteorology at the millenium*, R. P.
221 Pearce (Ed.), 2002, pp. 220–232 (Academic Press).
- 222 Yoshikawa, Y., and Masuda, A., Seasonal variations in the speed factor and deflection angle of
223 the wind-driven surface flow in the Tsushima Strait. *J. Geophys. Res.* 2009, **114**, C12022.